Conf-751101--60

PREPRINT UCRL- 76985

Lawrence Livermore Laboratory

MIRROR FUSION REACTOR STUDY

By Gustav A. Carlson and Ralph W. Moir

November 12, 1975

This paper was prepared for presentation at the American Nuclear Society Winter Meeting, November 16-21, 1975 in San Francisco, California

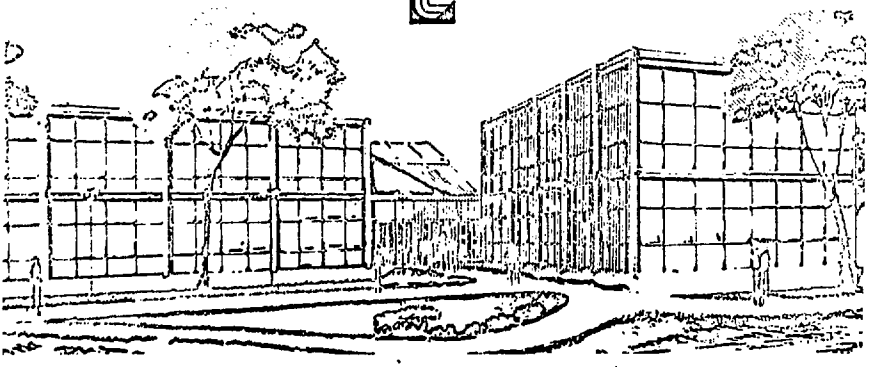

UCRL-76985

MIRROR FUSION REACTOR STUDY*

Gustav A. Carlson
Ralph W. Moir

ABSTRACT

The principal features of a fusion power reactor employing the magnetic mirror confinement concept are described. A parametric design and cost estimate analysis has been used to optimize the design for minimum capital cost per net electric output. Optimized parameters include the vacuum mirror ratio, the injection energy and angle, the choice of a thermal conversion cycle, and the design efficiency of the charged particle direct converter. The sensitivity of the cost of power for the optimized design to variations in many of the reactor parameters is discussed.

*Work performed under the auspices of the United States Energy Research & Development Administration under Contract No. U7405-ENG-48.

UCRL-76985

MIRROR FUSION REACTOR STUDY

Gustav A. Carlson
Ralph W. Moir

1. Introduction

A reference design study of a fusion reactor power plant employing the magnetic mirror confinement concept is underway at Lawrence Livermore Laboratory. It is our goal in this study to provide a conceptual engineering design for every essential reactor component. Furthermore, we are estimating the costs of all components which we believe will contribute significantly to the total plant cost. We are using a parametric design and cost estimate analysis to optimize the reactor design for minimum capital cost per net electric output.

Section 2 of this paper describes the principal features of our preliminary reactor design. Minor and even some major changes in these features are expected as a consequence of more detailed engineering design and the incorporation of the details into our parametric design and cost estimate analysis. Section 3 describes the parametric design and cost estimate analysis. Section 4 describes the detailed features of a design optimized for minimum capital cost per net electric output. Some of these detailed features can be expected to change as more complete design and economic data are added

to the analysis. Section 5 discusses the optimization of several key parameters, including the magnetic mirror ratio and the neutral beam injection energy, and illustrates the penalties for off-optimum design. Section 6 discusses the sensitivity of the cost of power for the optimized design to variations in some of the parameters which are either arbitrary (such as the physical size of the reactor) or incompletely known at this time. Examples of incompletely known parameters are the fraction of classically predicted confinement which will be achieved in mirror machines, the plasma density distribution and the degree to which it can be affected by coil design, and the practically achievable blanket energy multiplication.

2. Principal Reactor Features

Many of the principal features of our preliminary reactor design are illustrated in Figures 1-3. The superconducting magnet coil is of the Yin Yang configuration (see Fig. 1). This coil produces a magnetic field whose strength increases everywhere away from the center, i.e., a magnetic well. The superconductor will be multifilamentary niobium-tin embedded in copper stabilizer, and will operate at liquid helium temperature. The detailed section view in Fig. 1 shows the special coil and coil structure design developed for this reactor. The conductors are separated into two bundles, the inner "mirror coil" and the outer "main coil". Both conductor bundles have the full Yin Yang shape. The mirror coil is very close to the plasma while the main coil is further removed and has a much larger coil gap. A

result of this coil design is that the mirror point for the contained plasma is very near the inner edge of the total coil. The mirroring plasma extends only between the mirror coil windings and not between the main coil windings. This makes possible the use of an efficient, tension-type coil structure[1] to balance the enormous outward forces on the main coil windings. Only the mirror coil requires a less efficient clamp structure that does not intrude between the windings. The selection of the tension-type coil structure does require the use of selective leakage[2], i.e., spatial control of the mirror end losses, to prevent the impingement of escaping plasma ions on the tension structure. (Such impingement would result in an unacceptable heat load on the structure, an unacceptable gas load on the plasma, and a severe reduction in the power input to the direct converter.) Selective leakage is effected by providing local regions of reduced mirror field strength. In the present design the local *minima* are produced by lining the selective leakage ports with ferromagnetic iron (see Fig. 1).

Figure 2 shows the spherical shell blanket design. An advantage of the spherical design over earlier blanket designs for mirror machines is that it has a much more uniform first wall neutron loading. (Earlier mirror machine blanket designs were required to permit removal of blanket modules through the mirror coils[3], or to permit the flow of liquid lithium coolant along magnetic field lines[4]. In the present design the first requirement is made impossible by the coil and coil structure design, and the second requirement is circumvented by the use of helium coolant.)

The spherical shell completely surrounds the plasma except for slots at the mirrors and holes for the neutral beam injectors. Coolant manifolding encircles the shell at its equator. The shell is made up of modules resembling the sections of an orange (see Fig. 2). Lining the inner surface of each module is an array of submodules, similar to those described in our hybrid reactor design[3], but in this case containing no uranium. The submodules contain $LiAlO_2$ in particle form for the breeding of tritium, and a large amount of beryllium for neutron multiplication.

Figure 3 (as well as Figs. 1 and 2) shows the vertical orientation of the z axis of the reactor. (By definition, the z axis passes through both mirrors of a mirror machine.) We believe that the vertical orientation has structural and maintenance advantages compared to some earlier designs with horizontal orientation. In the present design the vertical orientation is essential to the proposed method of blanket module access. We propose to float the lower half of the reactor in a water-filled drydock. For blanket module access the lower half of the reactor is lowered in the drydock, exposing the spherical shell blanket as depicted in Fig. 3. This permits entry of a crane which lifts a blanket module (orange slice shape) directly upward and transports it away. Variations of this blanket access method, including the possibility of removing blanket modules without separating the reactor halves, are under investigation.

The mirror-confined plasma is sustained by energetic neutral beams of deuterium and tritium. For this reactor we have chosen the negative

ion acceleration method for the neutral beam injectors because of the high efficiency theoretically attainable at the desired injection energies.[5] Each injector module consists of a positive ion source with extraction grid, a cesium cell to convert positive ions to negative, a negative ion accelerator, a photodetachment electron stripping cell to convert accelerated ions to neutrals, and an inline beam collector to directly recover the energy of the unstripped negative ions.[6] Cryopanel gas pumping surfaces line the inner surfaces of the accelerator and the beam collector. There are four locations for injection between the two separate coils, two on the top half of the reactor, and two on the bottom half. The angle of injection relative to the field lines and the injection energy are design variables.

A direct energy converter is used to efficiently convert the power of the mirror end losses into electricity. In this design, the selective leakage necessitated by the tension-type coil structure makes possible the use of a multichannel direct converter, a feature which reduces its size and cost. Figure 3 depicts an eight channel direct converter coupled to the top half of the reactor through eight selective leakage ports. (There is an identical direct converter on the bottom half of the reactor. However, we are considering designs with direct conversion on only one end of the reactor.) The direct converter itself is a stacked array of flat, fan-shaped magnetic expanders terminating in a 4-stage collector which utilizes space charge blowup to separate and collect the various energy-group ions[7]. The collectors operate at high temperature, and thermal energy deposited by the impacting ions is transported to the reactor thermal conversion system. Cryopanel gas

pumping is provided in the collector region to remove the gas refluxed from the collectors. These cryopanels (as well as those in the neutral beam injectors) must be periodically defrosted to recover the deposited deuterium and tritium. Variations of this direct conversion design as well as entirely different direct converters, such as the two-stage Venetian Blind converter[8], are also being considered.

The reactor thermal conversion system converts the thermal energy of the blanket and the thermal energy from the direct converter into electricity. For this design we are proposing the use of a potassium Rankine cycle topping a high temperature steam cycle[9]. We predict that the increased conversion efficiency of this binary cycle will more than compensate for its higher capital cost.

3. Parametric Design and Cost Estimate Analysis

In order to be a good predictor for optimizing a fusion reactor design for minimum power cost, the parametric analysis must include a complete and accurate description of the plasma physics, the engineering, and the economics. The parametric analysis which we describe here is in a stage of evolution somewhat short of the ideal goals of completeness and accuracy. However, we believe that our analysis is developed to a state where it is extremely useful as a design tool. Our analysis has been computer programmed to permit rapid evaluation of parameter changes and alternative design concepts. In the following paragraphs we will describe the present version of our analysis, roughly in the order in which the computer program proceeds. We will identify our sources of data, assumptions, and scaling laws as we go along. Independent variables for which values must be provided to the program will be

identified as input.

First we input the physical size of the Yin Yang coil (L - distance between coil midpoints), the desired vacuum mirror ratio, the maximum conductor field strength and average current density, and estimates of $B_{conductor}/B_{mirror(max)}$ (a measure of coil magnetic efficiency) and $B_{mirror(max)}/B_{mirror(min)}$ (a measure of the depth of the selective leakage minima). The last two inputs are obtained from a detailed coil and selective leakage design[10]. Using this information and scaling laws developed from a series of coil design calculations using MAFCO[11], we roughly design the coil. We calculate the conductor geometry, the current required, and the position of the last closed $|B|$ contour (which defines the size of the magnetic well, and thus the size of the confined plasma).

Next we input the desired injection angle (90° is perpendicular to the magnetic field lines and thus the farthest from the loss cone.) The program contains a table of the stability-limited $\beta_\perp$ (perpendicular plasma pressure divided by total perpendicular pressure including the magnetic field) as a function of vacuum mirror ratio and injection angle. The table data are the predictions of a series of Fokker-Planck calculations[12]. The maximum stable β increases with increasing mirror ratio but decreases with increasing injection angle. Using the table ("using the table" in this discussion means interpolating for a specific case) gives us our β limit and permits the calculation of the reduced magnetic field strength within the diamagnetic plasma.

Next we input the desired injection energy for deuterium. (We assume that tritium is injected at the same velocity as the deuterium to achieve equal plasma penetration). Using tables of the DT reaction rate

$\overline{\sigma v}$ (a function of injection energy)[13] and the containment parameter $n\tau$ (a function of mirror ratio, injection energy, and injection angle)[12] we calculate Q, the ratio of fusion power to injected power. Q is proportional to the product of $\overline{\sigma v}$ and $n\tau$ divided by the injection energy. $\overline{\sigma v}$ has a maximum at an injection energy of about 100 keV. $n\tau$ increases as the 3/2 power of injection energy, and also increases with increasing mirror ratio and injection angle (as predicted by Fokker-Planck calculations)[12]. Thus, Q increases with mirror ratio and injection angle and maximizes at some injection energy above 100 keV. Typically, the fall-off in Q at energies above its maximum is slight.

At this point we also calculate the central plasma density, n_o, which is proportional to the product of β and the square of the central vacuum magnetic field strength divided by the injection energy. The proportionality constant depends on the relation between perpendicular plasma pressure ($P_\perp$) and injection energy, which is predicted by the Fokker-Planck calculations[12]. Then, using estimates of the axial and radial density distributions we calculate the total fusion power. (The axial density distribution comes from a combination of Fokker-Planck calculations, which give n vs. B, and MAFCO calculations, which give B vs. z. The radial density distribution comes from plasma buildup calculations). For a given density distribution, the total fusion power is proportional to $n_o^2 \overline{\sigma v} r_p^2 L$, where r_p is the midplane plasma radius (determined by the position of the last closed |B| contour.)

The required injected power is just P_{fusion}/Q. In order to calculate the required input power to the injector, we must know its efficiency. For the presently proposed negative ion injector system the program uses a derived scaling law[6] that predicts efficiency increasing

with injection energy.

We now input the neutron energy multiplication factor for the proposed blanket, M, and the energy conversion efficiencies of the proposed thermal and direct converters, η_{TH} and η_{DC}, respectively. (Different η_{TH} may be input for the main thermal plant and the bottoming cycle for the direct converter.) All of the power flows in the reactor system are now calculated. The input power to the injector and the auxiliary power (principally refrigeration power for the cryogenic coil) are subtracted from the gross electrical power to yield the net electrical power. The system efficiency is calculated as the ratio of net electrical power to total nuclear power (fusion plus blanket energy multiplication). The recirculating power fraction is calculated as the sum of the input power to the injector and the auxiliary power divided by the gross electrical power.

Now we begin the cost estimate. The reactor components for which separate capital costs are calculated are the magnet, the injector, the direct converter, the thermal converter, the blanket, the magnet shield (placed between the blanket and the coils to limit energy deposition in the coils), and the buildings and facilities. Indirect costs (engineering, and taxes, insurance, and interest during construction) are calculated as a fraction of the total capital cost (0.35 in the present program).

The magnet cost estimate is made up of 4 separate calculations. The conductor cost is calculated using an input value for the cost per ampere-meter of superconductor[14]. The cost of winding the coil is assumed to be proportional to the number of ampere-meters of conductor and is scaled from our hybrid reactor design[3]. The cost of the coil refrigerator

is also scaled from the hybrid design. The cost of the tension-type coil structure is taken to be proportional to the square of the conductor magnetic field strength and the square of the reactor length L, and is normalized to the estimated cost of a detailed single point design[10].

The injector system cost is assumed to be proportional to the input power to the injector and to the square root of the injection energy, and is normalized to the injector cost in the hybrid design[3]. The proportionality to power is based on the typical dominance of power supply costs in injector systems. The increase in injector cost with energy is due to the increased bulk and complexity of higher voltage systems. The accuracy of normalizing the injector cost to the hybrid injector is suspect because the hybrid injector was a quite different, positive ion acceleration design. More work is required on the injector cost estimate.

The 4-stage, stacked direct converter is designed based on the charged particle power into the converter, the injection energy, the number of direct conversion channels (an input variable), and the previously specified direct conversion efficiency. The estimated cost of the direct converter is calculated using scaling laws developed for 5 separate components of the converter: the vacuum enclosure, the vacuum pumping system, the expander magnet coil, the collectors, and the electrical equipment[7].

The cost estimate for the thermal converter is calculated using a unit cost in $/kw thermal, which is an input variable paired with the specified thermal system conversion efficiency[9].

The blanket cost is calculated using a unit cost in $/square meter of first wall area ($120K/$m^2$ for the beryllium-loaded blanket).

The magnet shield cost estimate is scaled from the hybrid design[3].

The reactor buildings and facilities cost is presently taken to be a constant $150M.

Finally, the cost of power ($/kwe) is calculated by dividing the total capital cost plus the indirect costs by the net electrical power.

4. Features of an Optimized Reactor

In this section we describe the detailed features of a reactor optimized for minimum capital cost per net electric output. A summary of the reactor features is given in Table 1 and a power flow diagram is given in Fig. 4. The information in this section and the parametric results discussed in subsequent sections were calculated using the present version of our computerized parametric design and cost estimate analysis. As stated previously, our computer model is an evolving design tool. We have already discovered inaccuracies and omissions in the present model which, when corrected, will affect our results. We will discuss these uncovered weaknesses as a guide to possible future changes in our design.

The physical size of the reactor is characterized by L, the distance between the midpoints of the two coils. In the present coil design, with its inward-shifted mirror points, the plasma length is less than L. For the design of Table 1, L = 20 m (plasma length ≈ 16 m). There is nothing optimum about this size; larger L's will result in higher power outputs at somewhat lower $/kwe. L = 20 m was chosen to yield a reactor with a net output comparable to present day power plants.

The Yin Yang magnet has an optimized vacuum mirror ratio of 2.5 and a maximum field strength at the conductor of 16 Tesla. As a consequence of the coil magnetic efficiency and selective leakage parameters, the mirror field which confines the plasma is

$$B_{mirror(min)} = 16/(1.13 \times 1.05) = 12.8 \text{ Tesla}$$

The central vacuum field is then

$$B_{0,vac} = 12.8/2.5 = 5.1 \text{ Tesla.}$$

The average current density specified for the coil was 2.5 kA/cm^2 and the predicted superconductor requirement was 1.7×10^{10} ampere-meters. More exact coil calculations[10] indicate that the actual ampere-meter requirement is probably about 30% higher than this, which will increase our predicted superconductor and coil winding costs.

The plasma radius, $r_p = 3.2$ m, is equal to the midplane radius of the magnetic well produced by the Yin Yang coil. The optimized deuterium injection energy is 200 keV and the optimized injection angle is 70°. The predicted overall injection efficiency (after credit is taken for energy recovery) is 83%. The plasma β (stability-limited) is 0.74, which results in a plasma mirror ratio,

$$R = \frac{R_{vac}}{\sqrt{1-\beta}} = 4.9$$

The central plasma density, n_o, is predicted to be 2.4×10^{14} cm^{-3} and the plasma fusion power is predicted to be 2030 Mw. Recently completed Fokker-Planck calculations[12] yield an n_o only 0.82 of this value. (The inaccuracy in our computer model was an underestimate of $P_\perp$ for a given injection energy.) Another inaccuracy, this one in our favor, was our estimate of the axial density profile. The combined Fokker-Planck and MAFCO calculations yielded a power proportionality constant 1.2 times higher than that used in our computer model. The combined effect of these two inaccuracies is to lower the predicted fusion power somewhat:

$2030(0.82)^2\ 1.2 = 2000$ Mw.

We neglect this correction in the following discussion.

The plasma containment parameter, $n\tau$, is predicted to be 4.8×10^{13} s/cm^3 and the resulting value for Q is 1.02.

The average blanket energy multiplication factor, M, is 1.7. This value is the result of a neutronic calculation[15] for a spherical blanket with 93% surface coverage (the spherical surface loses 6% to the mirror openings and 1% to the injectors). The composition of the blanket assumed for the neutronic calculation was 50 volume % beryllium, 20% $LiAlO_2$, 5% vanadium structure, and 25% helium coolant. The use of vanadium for the structural material is not crucial to the neutronic performance of the blanket. Another material may be chosen when the thermal-hydraulic-structural design of the blanket is carried out.

For a blanket thickness of 1.0 m and a required magnet shield thickness of 0.78 m, the present computer model calculated a first wall radius of 6.5 m. This, in turn, resulted in a calculated 14 MeV neutron wall loading of 3.1 Mw/m^2. However, we have discovered that the simplified model of the coil in our analysis underestimated the bulk of the coil. The first wall radius required by the detailed coil design appears to be about 5.2 m. This change in blanket location would increase the neutron wall loading to 4.8 Mw/m^2. We must consider the implications of this rather high wall loading in our blanket design and maintenance study. There is an economic trade-off between wall loading and down time for blanket replacement. If our wall loading is too high, we will have to lower the fusion power density (for example, by lowering the magnetic field strength), or increase the first wall radius relative to the plasma radius.

The thermal conversion system for the blanket heat is a potassium-topped steam cycle with an overall conversion efficiency, η_{TH} = 48% (already discounted for the pumping power of the primary helium coolant and the potassium and water working fluids). This thermal conversion system was found to be the optimum of the 3 systems we considered. The peak cycle temperature required for this system is 1100 K. This is probably unacceptably high for vanadium, a fact that must be considered in our detailed blanket design.

The thermal conversion efficiency for the direct converter heat, $\eta_{TH,BOT}$, is 40%.

The 4-stage direct converter is specified to have 16 channels (8 at each end of the reactor) and has an optimized conversion efficiency of 70%.

The net electric output of this optimized reactor is 890 Mw. The system efficiency is 28% and the recirculating power fraction (sum of the input power to the injector and the auxiliary power divided by the gross electrical power) is 0.73.

The total capital cost of the optimized reactor was calculated to be $2.4B. Thus, the capital cost per net electric output is $2700/kwe. The capital cost breakdown for the optimized reactor is shown in Table 2. (For the cost breakdown calculation the indirect costs were prorated among the reactor components.)

As mentioned previously, the cost estimate for the magnet conductor and winding labor is probably low due to a low estimate of

the amount of conductor required. Recently, more detailed consideration of the direct converter indicates that its cost estimate may be low by as much as a factor of 2. There is a sizable continuing effort on direct converter design and costing. Finally, the cost estimates for the injector and the buildings and facilities should be considered preliminary, in that detailed costing of these components is just beginning.

5. The Optimization Process

In the preceding description of an optimized reactor design we identified 5 optimized parameters: the vacuum mirror ratio, the injection energy, the injection angle, the thermal conversion efficiency, and the direct conversion efficiency. In this section we discuss the optimization of these 5 parameters and show the penalties for off-optimum design. In the discussions that follow we will describe the major influences on the results, but we will not attempt to include all the effects which are in our computer model.

R_{vac} Optimization. The central field strength decreases as the vacuum mirror ratio is increased (with the maximum conductor field strength held constant). This results in lower plasma density, fusion power, and net electric power. Consequently, the $/kwe costs of components such as the magnet, blanket, shield, and buildings and facilities increase with mirror ratio. On the other hand, the $/kwe costs of power handling components such as the injector, direct converter, and thermal converter decrease with increasing mirror ratio. This is because $n\tau$ (and hence Q) increases with mirror ratio, thus reducing the recirculating power fraction. Fig. 5 shows the $/kwe cost variation with R_{vac}. The minimum cost, $2700/kwe, occurs at $R_{vac} = 2.5$.

W_{inj} Optimization. Plasma density, fusion power, and net electric power also decrease with increasing injection energy, thus causing the \$/kwe cost of the magnet, etc., to increase. But the recirculating power fraction decreases with increasing injection energy because $n\tau$ (and Q) and the injector efficiency increase with W_{inj}. Thus, the \$/kwe costs of the power handling components decrease with increasing W_{inj}. Figure 6 shows the \$/kwe cost variation with W_{inj}. The minimum occurs at W_{inj} = 200 keV.

θ_{inj} Optimization. As the injection angle θ_{inj} is increased, the net electric power decreases because the stability-limited β decreases. However, $n\tau$ (and Q) increase with θ_{inj}. So again we see an optimum for minimum \$/kwe. Figure 7 shows the optimum to occur at $\theta_{inj} = 70°$.

η_{TH} Optimization. We have considered 3 different thermal conversion systems: a steam cycle with η_{TH} = 38% that costs \$70/kw handled, a potassium-topped steam cycle with η_{TH} = 48% that costs \$139/kw handled, and an advanced, higher temperature potassium-topped steam cycle with η_{TH} = 53% that costs \$374/kw handled. Figure 8 shows that the total \$/kwe cost of the reactor minimizes for the lower temperature potassium-topped steam cycle.

η_{DC} Optimization. The efficiency of the 4-stage direct converter can be increased by design changes which make the direct converter larger and more expensive. Figure 9 shows that the total \$/kwe cost of the reactor minimizes for a direct conversion efficiency of 70%.

6. Sensitivity Study of Various Parameters

In this section we discuss the sensitivity of the net output power, total cost, and total \$/kwe cost of the optimized reactor to variations in a number of parameters. We varied only one parameter at a time, holding

all others constant, including the 5 optimized parameters discussed in the preceding section. In a few cases, the optimum design point shifts somewhat for the extreme parameter variations.

L Variation. Figure 10 shows the sensitivity of the reactor net power and cost to the distance between the midpoints of the two coils, L. (In all of the Figures in this section, the optimized design of Table 1 is indicated by a circle.) Some reduction in the $/kwe cost could be achieved with L's larger than 20 m, but the potential improvement is not large. Smaller machines will cost considerably more in $/kwe, but may be attractive as experimental reactors because of their lower dollar cost. For example, a machine with L = 10 m is predicted to cost only $500M (as compared to $2.4B for L = 20 m). A machine with L = 14 m is predicted to cost $1B. For the present design, L = 10 m is a lower limit below which the blanket and shield will not fit between the plasma and the coil. The requirement that alpha particles be adiabatically contained sets another limit on minimum length. Preliminary estimates indicate that this lower limit is less than 20 m, but how much less is uncertain.

Reoptimization of the reactor for the extreme values of L yields somewhat different results than the solid curves of Fig. 10. The reoptimized design points for L = 10 m and L = 28 m are shown as triangles on Fig. 10. At L = 10 m the optimum R_{vac} is 2.1; at L = 28 m the optimum R_{vac} is 2.8.

Variation of $Q/Q_{Classical}$. Figure 11 shows the sensitivity of the $/kwe cost of the reactor to $Q/Q_{classical}$. Our optimized design assumed $Q = Q_{classical}$. If anomalous losses result in lower Q's, the recirculating power fraction rises toward unity and the $/kwe cost increases steeply. On the other hand, if the classical Q could be exceeded by a factor of 2, the

cost of power would drop from \$2700/kwe to \$1500/kwe. Reoptimization of the reactor $Q/Q_{classical} = 2$ results in a further reduction of the cost of power: \$1400/kwe at a new optimum $R_{vac} = 2.2$. There are a number of effects not now included in the calculation of the classical Q; some of these will lower Q and some will raise it. Our reactor would benefit greatly from new mirror containment ideas (or old ideas reinvestigated) which would raise Q from the classical values we are using.

Fusion Power Variation. As described previously, the amount of fusion power produced in the reactor depends on many things, some of which are incompletely known at this time (for example, the plasma density distribution). Furthermore, we are investigating coil modifications that will increase the plasma volume (and hence the fusion power). One possibility is a Yin Yang coil pair with tapered gaps, i. e., coil gaps that increase circumferentially from the Z-axis to the turnarounds. This modification increases the radius of the last closed $|B|$ contour. Elongating the coils can further increase the fusion power (although this modification would also increase the coil cost, an effect that is not included in the following discussion). Figure 12 shows the sensitivity of the reactor net power and cost to the "fusion power multiplier", which is unity for our optimized design of Table 1. We see that the \$/kwe cost of the reactor would increase sharply for multipliers less than unity. For multipliers greater than unity, the \$/kwe cost decreases. For a multiplier of 3.5 the cost of power has dropped to \$2400/kwe. Furthermore, a reoptimization for this case yields a new optimum R_{vac} of 3.0 (instead of the previous 2.5) and an optimized power cost of \$2000/kwe.

B_{cond} Variation. The maximum conductor field strength, $B_{cond} = 16$ Tesla, was chosen for our optimized design of Table 1 based on our expectations for superconductor development. Figure 13 shows the

sensitivity of the reactor net power and cost to B_{cond}. (For these calculations we did not change the estimated $/ampere meter cost of the conductor as a function of B_{cond}. For all cases the conductor cost used was $.0056/ampere meter.) We see that at 16 Tesla we are beyond the knee of the curve, and that further increases in field strength result in only modest reductions in the $/kwe cost. The improvement would be even less if the higher field conductor is more expensive per ampere meter. A decrease in B_{cond} was mentioned previously as a way to decrease the neutron wall loading. For changes in B_{cond} alone, the neutron wall loading varies linearly with the reactor net power. So, from Fig. 13, we could halve the neutron wall loading by reducing B_{cond} from 16 Tesla to 13.5 Tesla, but the penalty is an increase in the cost of power from $2700/kwe to $3400/kwe.

M Variation. Figure 14 shows the sensitivity of the reactor net power and cost to the blanket energy multiplication factor, M. The $/kwe cost increases sharply as M is reduced below the 1.7 value used in our optimized design. For M = 1.2, a value which can be achieved with no beryllium, the cost of power is $4600/kwe.

Variation of the Number of Direct Converter Channels. Figure 15 shows the sensitivity of the $/kwe cost of the reactor to the number of channels in our 4-stage direct converter. (The number of channels is equal to the number of selective leakage ports.) The cost of power is fairly insensitive to this parameter until the number of channels drops below about 10 .

Clamp-Type Coil Structure. We investigated the use of the clamp-type coil structure from the hybrid reactor design instead of the tension-type structure. However, we retained selective leakage since the 4 channel direct converter requires it. A reoptimization of the

reactor resulted in the same optimized parameters as before (R_{vac}, W_{inj}, etc), but an increased cost of power ($3200/kwe vs. the previous $2700/kwe).

Positive Ion Injector System. Finally, we investigated the use of a positive ion injector system such as that used in the hybrid reactor design. The maximum efficiency of the positive ion injector system is 73% and occurs at an injection energy of 70 keV. At energies above 100 keV, the injection efficiency falls rapidly. A reoptimization of the reactor with a positive ion injector system resulted in new optimized values for R_{vac} (4.25), W_{inj} (100 keV), and θ_{inj} (60°). The cost of power for this optimized design is $5100/kwe.

7. Conclusions

The parametric analysis which we have described helps us choose near-optimum parameters for our mirror reactor reference design study now underway. Our sensitivity study helps identify critical areas where design effort should be concentrated to improve reactor performance and identifies areas with little to be gained.

We believe a mirror reactor will work if the components which handle recirculating power, particularly the injector and direct converter, can be made to work efficiently, and if the plasma is sufficiently stable so that the confinement is essentially classical. We believe we have conceptual solutions to all of the major technological problem areas, including start-up, steady state fueling, impurity control, remote maintenance, and blanket replacement. The predicted cost of power production for our preliminary optimized reactor is $2700/kwe, which is considerably higher than present day nuclear plant costs. Fundamentally, our cost is high because of our high recirculating power fraction. Our

cost would be reduced most markedly by an increase in plasma Q.

Our on-going design study will end in a reference reactor design ($\sim$ June, 1976). We request and would appreciate comments and critique concerning this work.

REFERENCES

1. M. A. Peterson, R. W. Werner, M. A. Hoffman and G. A. Carlson, "A Modularized Mirror Fusion Reactor Concept with Emphasis on Fabricability, Assembly, and Disassembly," LLL report UCRL-75826, Rev. 1, May 1975. Also M. A. Peterson, unpublished work in progress.

2. G. A. Carlson, "Selective Leakage of Charged Particles in Mirror Machines," LLL report UCRL-51434, July 1973.

3. R. W. Moir et al, "Progress on the Conceptual Design of a Mirror Hybrid Fusion-Fission Reactor," LLL report UCRL-51797, June 1975.

4. R. W. Werner et al, "Progress Report #2 on the Design Considerations for a Low Power Experimental Mirror Fusion Reactor," LLL report UCRL-74054-2, 1973.

5. J. Hovingh and R. W. Moir, "Efficiency of Injection of High Energy Neutral Beams into Thermonuclear Reactors," LLL report UCRL-51419, 1973. Also J. H. Fink, "Power Efficiencies of Neutral Beam Systems," LLL report UCRL-51650, September 1974.

6. J. H. Fink, "Photodetachment of Electrons from Negative Ions in a 200-keV Neutral Deuterium-Beam Source," LLL report UCID-16844. Also J. H. Fink, unpublished work in progress.

7. W. L. Barr, LLL unpublished work in progress.

8. R. W. Moir, W. L. Barr, and G. A. Carlson, "Direct Conversion of Plasma Energy to Electricity for Mirror Fusion Reactors," LLL report UCRL-76051, September 1974.

9. R. J. Rossbach, "Potassium Topping Cycles for Stationary Power," NASA report CR-2518, March 1975.

10. M. A. Peterson, LLL unpublished work in progress.

11. W. A. Perkins and J. C. Brown, "MAFCO--A Magnetic Field Code for Handling General Current Elements in Three Dimensions," LLL report UCRL-7744-Rev. 2, November 1966.

12. M. E. Rensink et al, "Some Recent Computational Results on Mirror Confinement," LLL report UCID-16459, March 1974 and "Theoretical Studies of Plasma Confinement in Magnetic Mirrors," LLL report UCRL-75993, September 1974. Also M. E. Rensink, LLL unpublished work in progress.

13. R. W. Moir, "Conceptual Design Considerations for D-T Mirror Reactors With and Without a Fission Blanket," LLL report UCRL-75596, April 1974.

14. D. N. Cornish and R. Scanlon, LLL unpublished work in progress.

15. J. D. Lee, LLL unpublished work in progress.

TABLE 1 -- FEATURES OF AN OPTIMIZED REACTOR

Size

$L = 20$ m

Magnet

$R_{vac} = 2.5$ (optimum)

$B_{cond} = 16$ T

$B_{cond}/B_{m(max)} = 1.19$

$B_{m(max)}/B_{m(min)} = 1.05$

$j = 2.5$ kA/cm^2

conductor required = 1.7×10^{10} Ampere-meters

Plasma

$r_p = 3.2$ m

$W_{inj} = 200$ keV (optimum)

$\theta_{inj} = 70°$ (optimum)

$\beta = 0.74$

$R = 4.9$

$n_o = 2.4 \times 10^{14}$ cm^{-3}

fusion power = 2030 Mw

$n\tau = 4.8 \times 10^{13}$ s/cm^3

$Q = 1.02$

$r_p/r_{larmor} = 92$, $L/r_{larmor} = 570$

Injector

$\eta_{INJ} = 0.83$

Blanket and Magnet Shield

$M = 1.7$

Blanket thickness = 1.0 m

Shield thickness = 0.78 m

Neutron wall loading = 3.1 Mw/m^2

Thermal Conversion

$\eta_{TH} = 0.48$ (optimum)

$\eta_{TH,BOT} = 0.40$

Direct Conversion

16 channels

$\eta_{DC} = 0.70$ (optimum)

Net Electric Power = 890 Mw

$\eta_{SYS} = 0.28$

Recirculating Power Fraction = 0.73

Total Capital Cost = $2.4 B = $2700/kwe

TABLE 2 -- CAPITAL COST BREAKDOWN FOR THE OPTIMIZED REACTOR

Magnet	14%	Conductor	39%
		Winding Labor	16
		Structure	31
		Refrigerator	14
			100%
Direct Converter	15%	Tank	18%
		Vacuum System	25
		Expander coil	20
		Collectors	29
		Electrical	8
			100%
Injector	28		
Thermal Converter	27		
Blanket	4		
Magnet Shield	4		
Buildings and Facilities	8		
	100%		

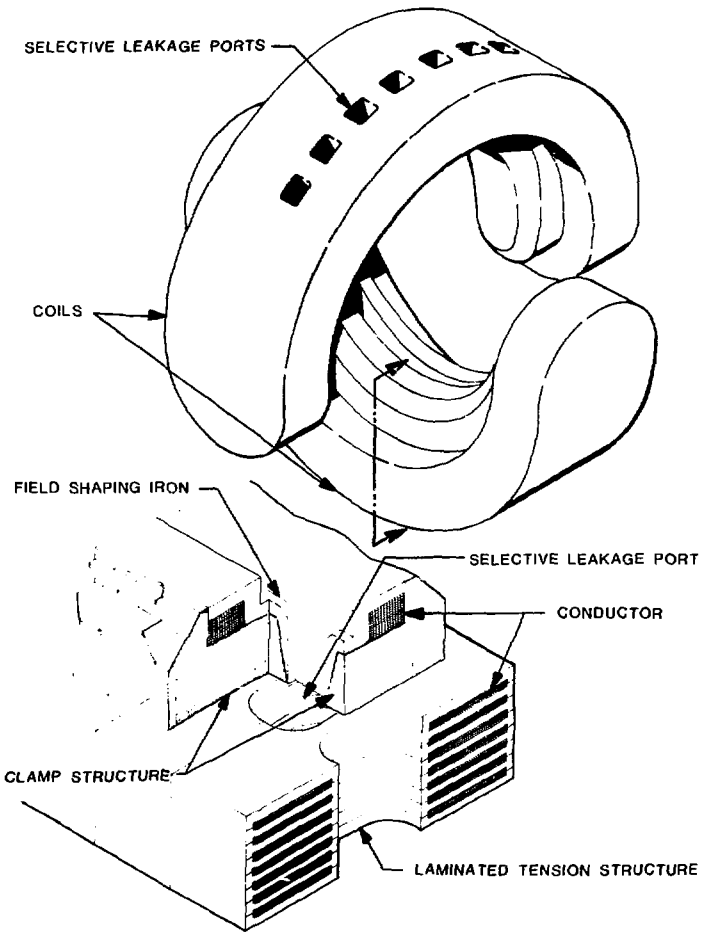

Fig. 1 -- Yin Yang Coil and Coil Structure

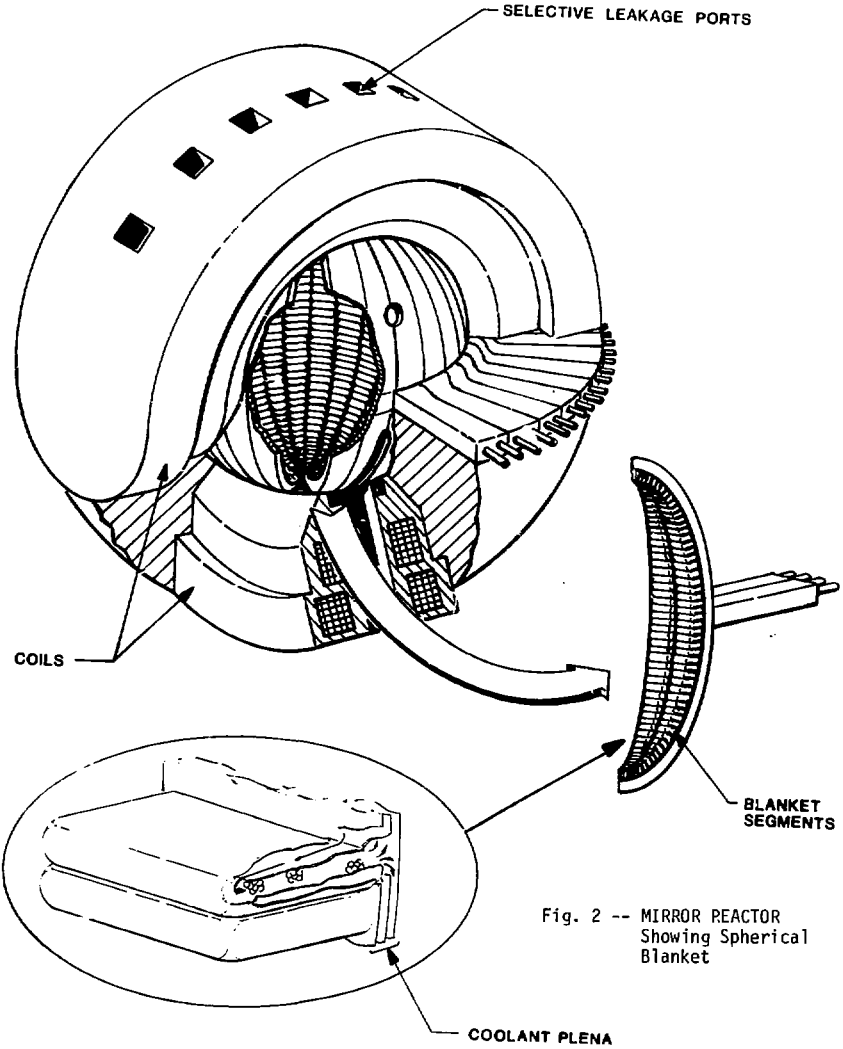

Fig. 2 -- MIRROR REACTOR Showing Spherical Blanket

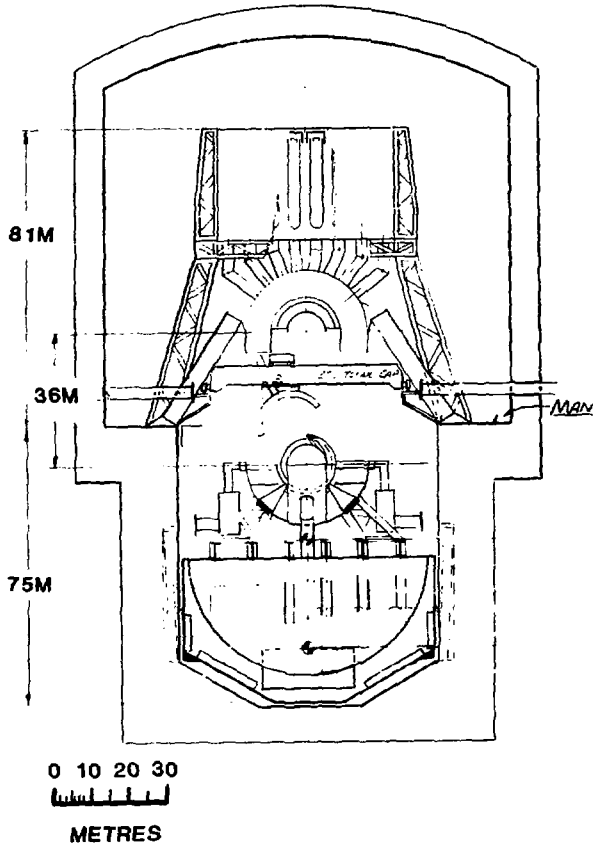

REACTOR - OPENED POSITION

Fig. 3

POWER FLOW DIAGRAM

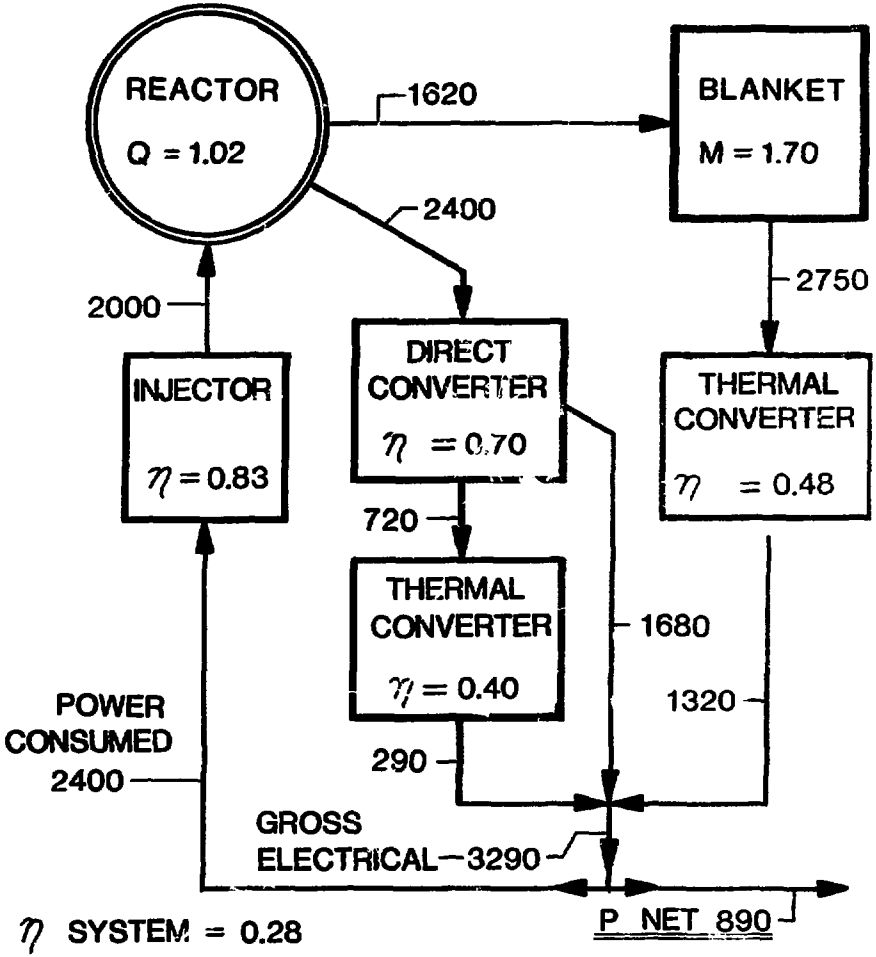

η SYSTEM = 0.28

$$\text{RECIRCULATING POWER FRACTION} = \frac{\text{POWER CONSUMED}}{\text{GROSS ELECTRICAL}} = 0.73$$

Fig. 4

POWER IN MEGAWATTS

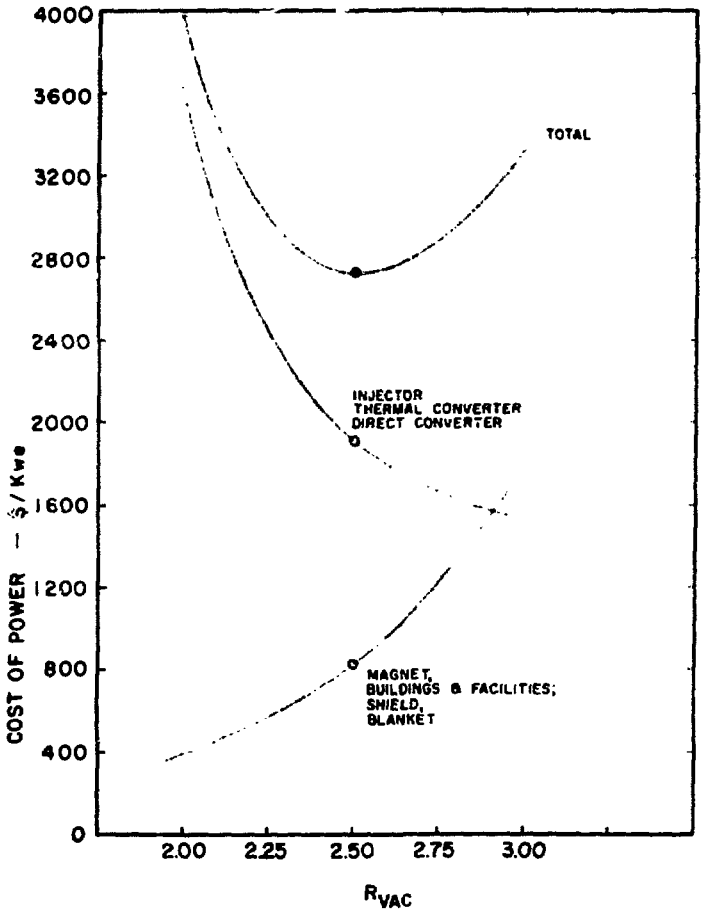

Fig. 5 -- Optimization of Vacuum Mirror Ratio

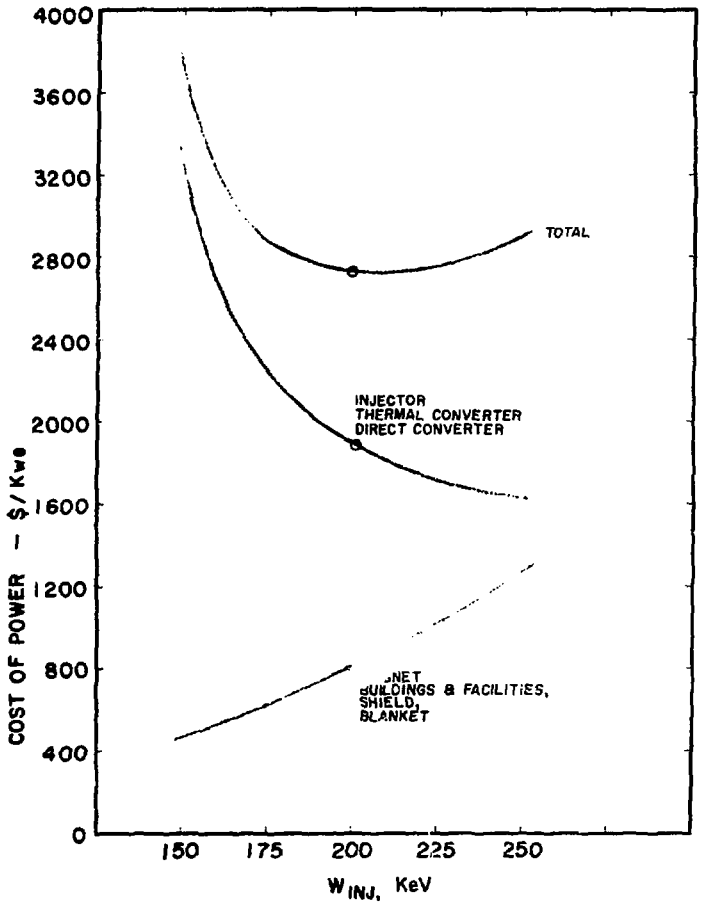

Fig. 6 -- Optimization of Injection Energy

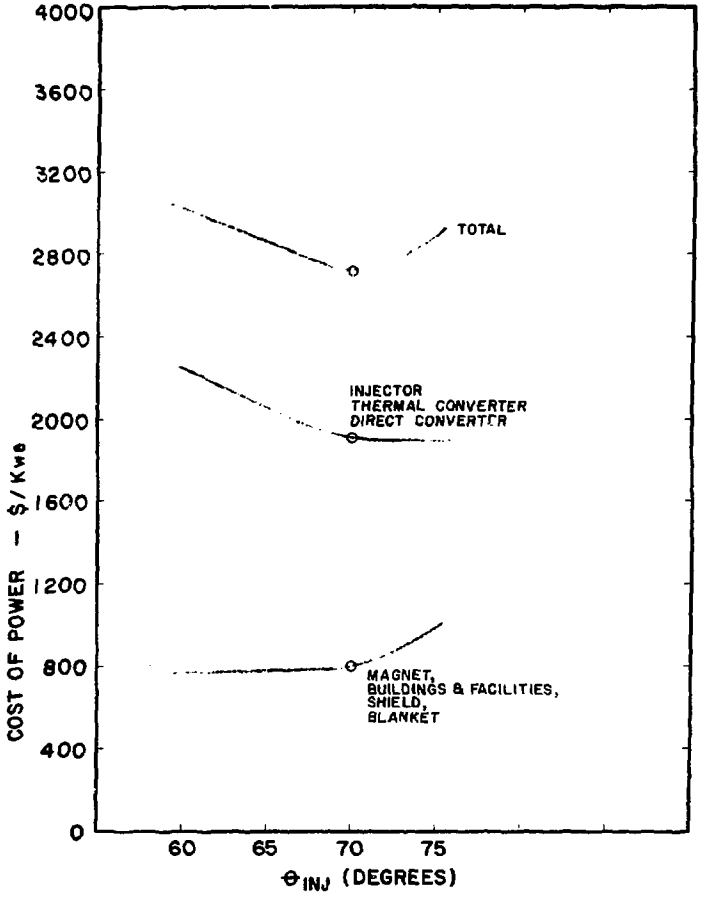

Fig. 7 -- Optimization of Injection Angle

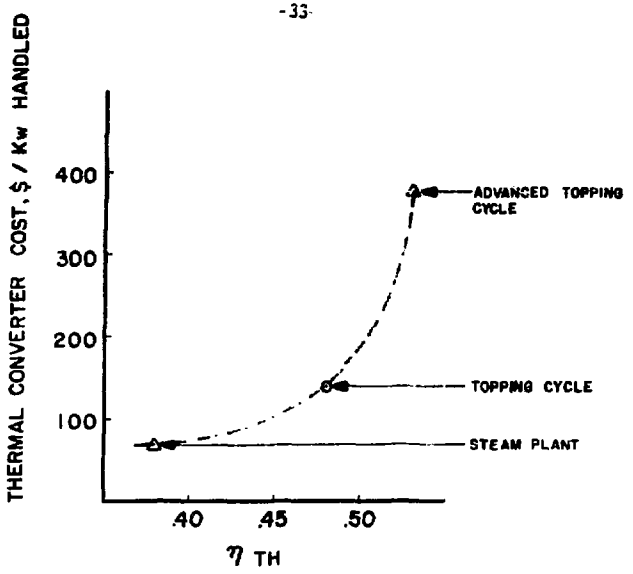

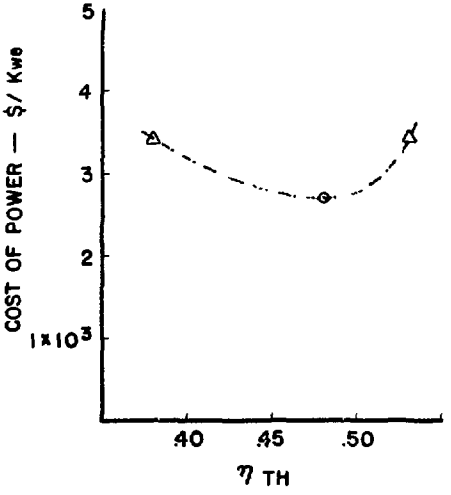

Fig. 8

Thermal Converter Optimization

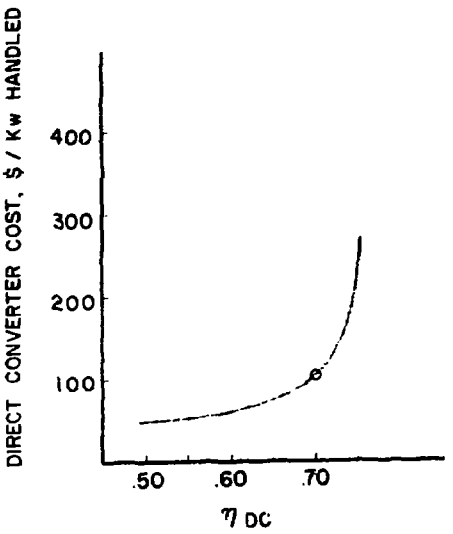

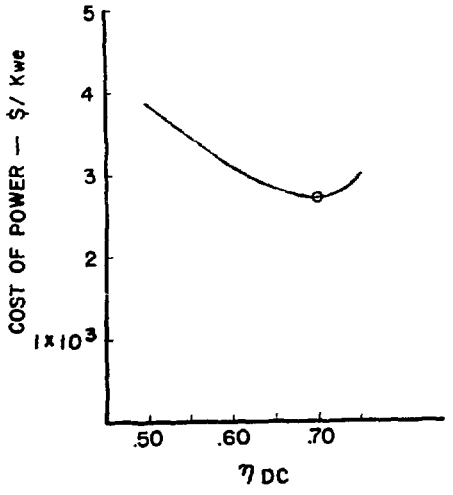

Fig. 9
Direct Converter Optimization

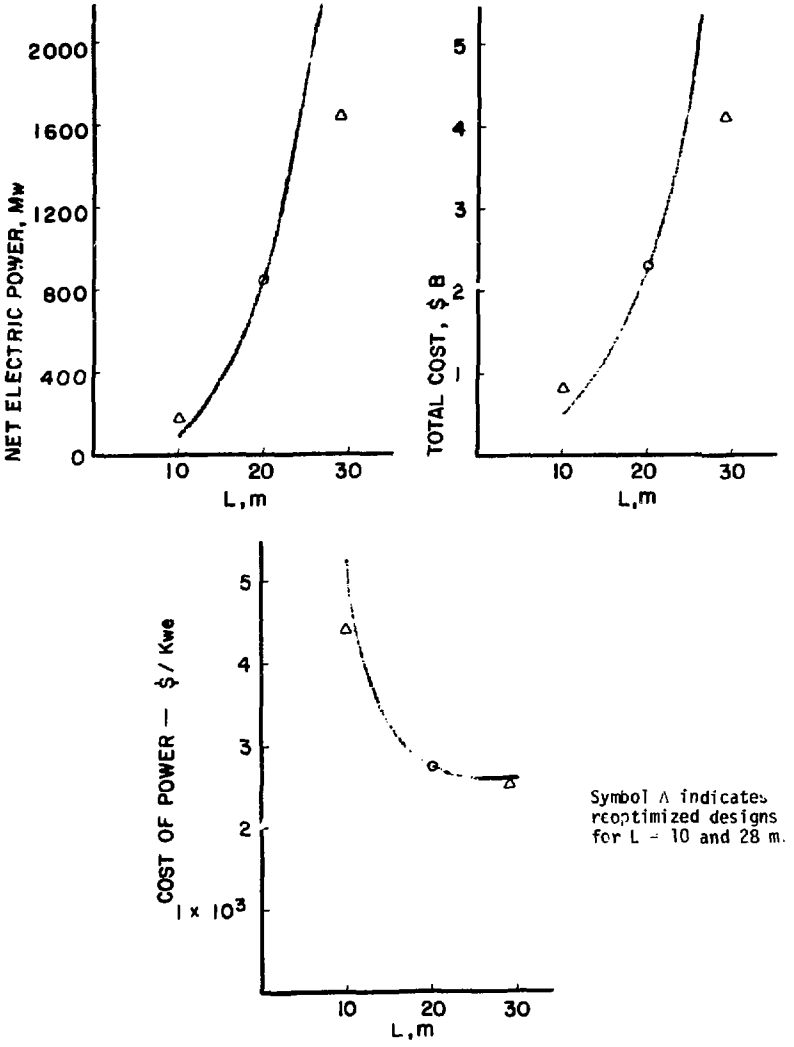

Symbol Δ indicates reoptimized designs for L = 10 and 28 m.

Fig. 10 -- Variation of Reactor Length

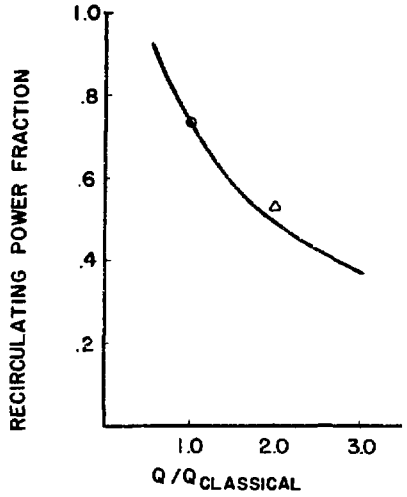

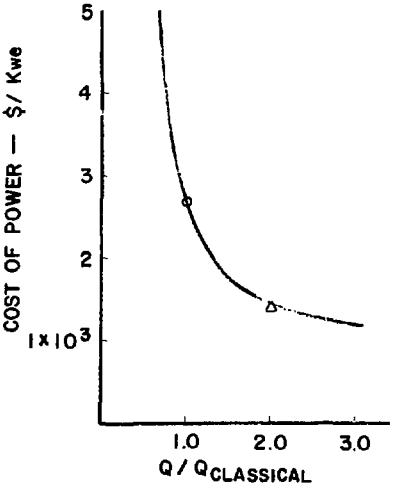

Symbol Δ indicates reoptimized design for $Q/Q_{classical} = 2$.

Fig. 11 -- Variation of $Q/Q_{Classical}$

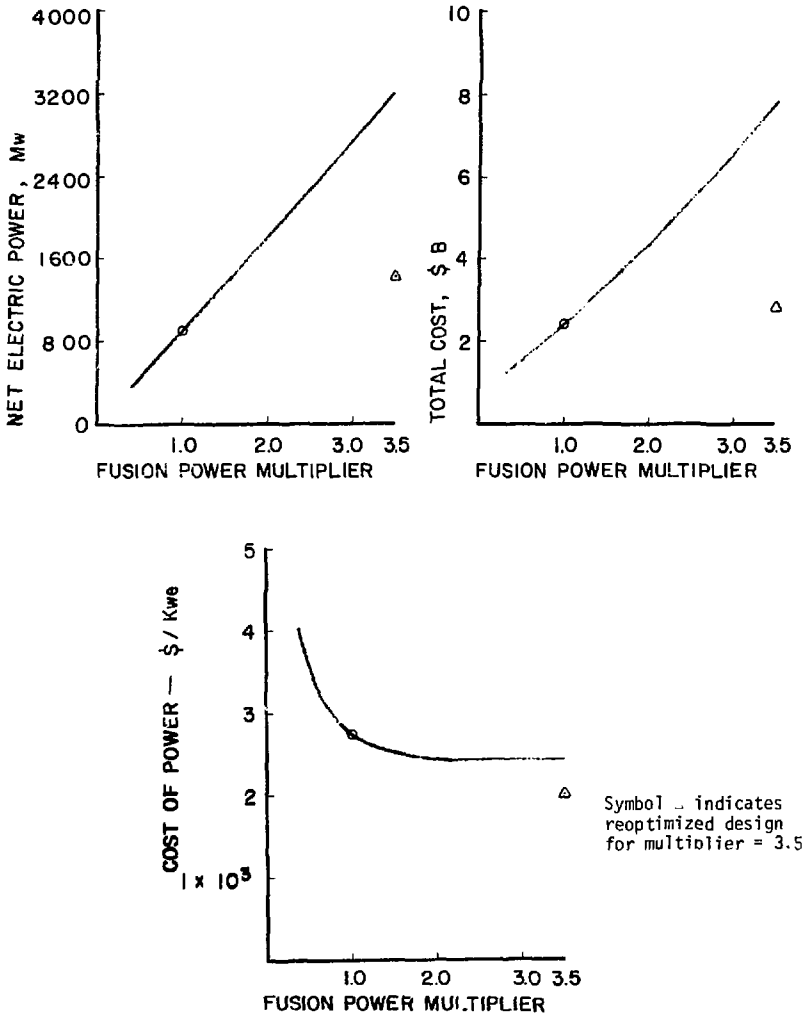

Fig. 12 -- Fusion Power Variation

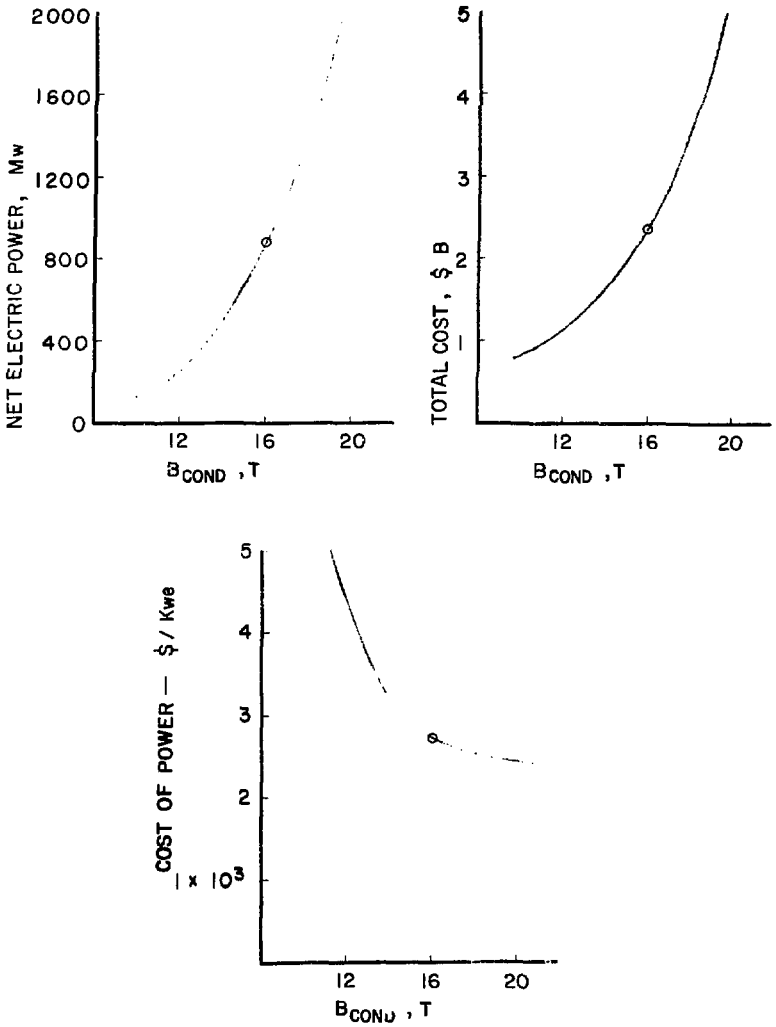

Fig. 13 -- Variation of Conductor Field Strength

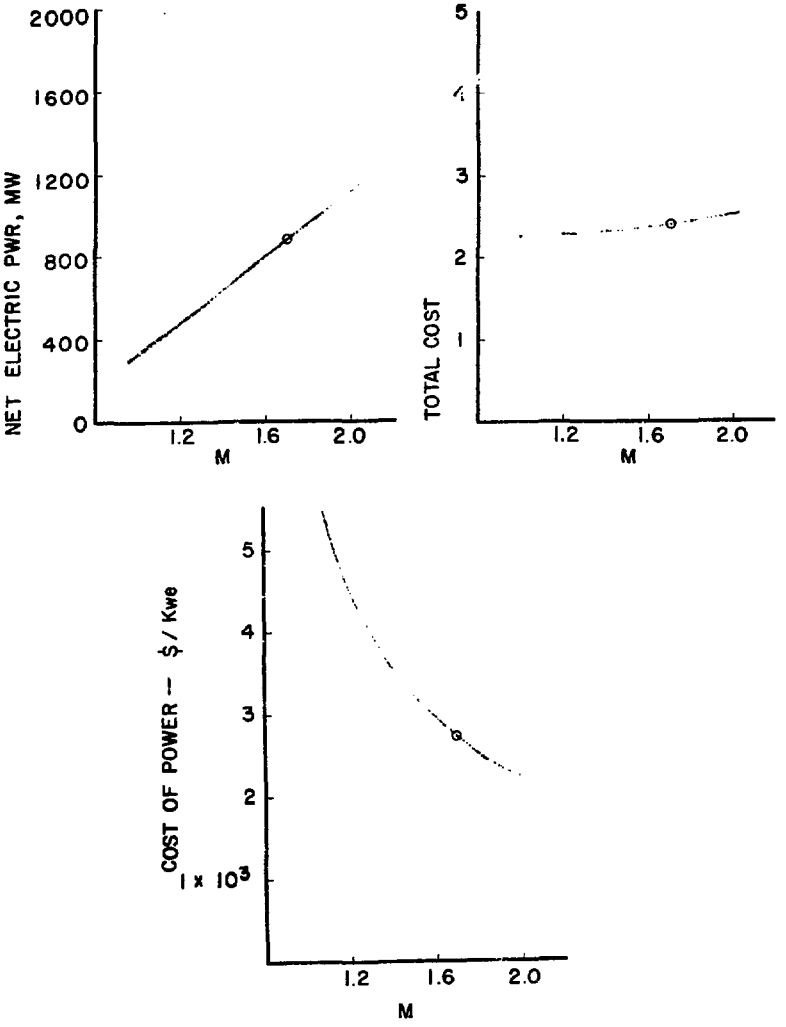

Fig. 14 -- M Variation

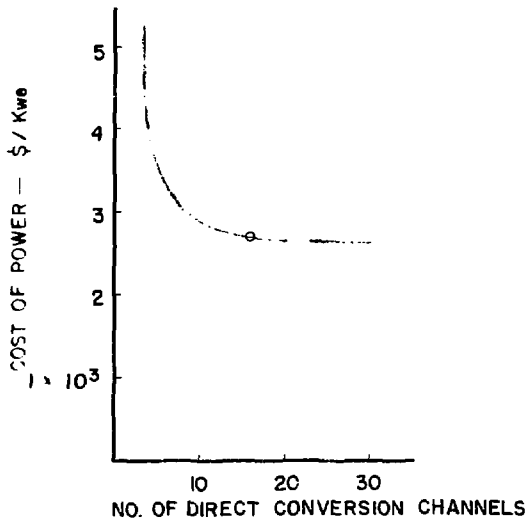

Fig. 15 -- Variation of the Number of Direct Conversion Channels